

Changes of the optical spectrum of the hypergiant ρ Cas due to a shell ejection in 2013

V.G. Klochkova, V.E. Panchuk, and N.S. Tavalzhanskaya

Special Astrophysical Observatory RAS, Nizhnij Arkhyz, 369167 Russia

August 2, 2018

Abstract Spectral monitoring of the yellow hypergiant ρ Cas with the by 6-m telescope of the Special Astrophysical Observatory with a spectral resolution of $R \geq 60\,000$ has led to the detection of new features in the kinematic state of its extended atmosphere following the ejection of matter in 2013. Significant changes in the profile of the $H\alpha$ line were detected: the line had a doubled core for the first time in a 2014 spectrum, an inverse P Cygni profile on December 13, 2017, and the profile was again doubled on August 6, 2017 and September 5, 2017, but was strongly shifted toward longer wavelengths, indicating a rapid infall of matter. Splitting of the profiles of strong, low-excitation absorptions into three components was first detected in 2017. There is no correlation between the evolution of the profiles of $H\alpha$ and the splitted absorptions. Pulsation-like variability with an amplitude of about 10 km/s is characteristic only of symmetric weak and moderate-intensity absorption lines. Shell emissions of iron-group elements can be identified in the long-wavelength part of a spectrum obtained in 2013, whose intensity decreased until they completely disappeared in 2017. In the absence of emission in the cores of the H and K lines of Ca II, emissions of shell metals are visible in the wings of these lines.

Keywords: massive stars, evolution, hypergiants, shell ejections, optical spectroscopy.

1. Introduction

The cool, extremely luminous star ρ Cas (Sp=G2 Iae) belongs to a small group of rare yellow hypergiants. The topical nature of a detailed study of these objects is due to the fact that such massive stars are the most probable progenitors of Type II supernovae (SN II). Moreover, hypergiants are evolutionarily related to extremely luminous variables such as η Car. In the Hertzsprung–Russell (hereafter HR) diagram hypergiants are close to the luminosity limit of the instability strip for A–M stars [1–3]. In addition to their high luminosities, yellow hypergiants differ from ordinary supergiants in the high rate of their mass loss via their stellar winds and the presence of gaseous–dusty circumstellar shells. The instability of hypergiants is manifest through weak brightness variability (with amplitudes $\approx 0.2 \div 0.4^m$), usually referred to as pulsations. The nature of the pulsations of massive stars in the stage of contraction of the helium core has been studied by Fadeev [4], who concluded that long-period, radial pulsations in ρ Cas have a low probability.

Along with the above manifestations of instability, yellow hypergiants also undergo sporadic variations, called “shell episodes”, when the star loses mass especially intensively, becoming enveloped in cool, ejected matter forming a pseudo-photosphere for several hundred days. Note that the term “flare” is used in the Russian literature rather than the English “outburst”; this is not logical, since

the brightness of the star drops significantly during the ejection of the shell. It would be more correct to use the terms “eruption” or “ejection”. In the case of ρ Cas, the last event of this kind occurred in 2000–2001, when the star lost up to $3 \times 10^{-2} \mathcal{M}_{\odot}$ [5] and its brightness decreased by 1^m . Despite its significant loss of mass (the mass-loss rate reaches $10^{-4} \mathcal{M}_{\odot}/\text{yr}$), unlike other yellow hypergiants, ρ Cas lacks circumstellar dust (see [6] and references therein). No extended circumstellar structure has been detected, and the star appears point-like even when observed with high spatial resolution by the Hubble Space Telescope [7]. At the same time, a thin circumstellar gas envelope is present, and is fairly structured, as is shown by CO observations [8, 9].

In the HR diagram, ρ Cas is located at the boundary of the Yellow Void [1], separating hypergiants and luminous blue variables (LBVs) in their quiescent phase. The amplitudes of pulsations of yellow hypergiants apparently increases sharply at the boundary of the Yellow Void, increasing the instability of their atmospheres and leading to shell ejection [1]. The results of long-term spectral monitoring [10–13] of V1302 Aql, which is a close relative of ρ Cas, are relevant here. This yellow supergiant, associated with the powerful IR source IRC +10420, traversed a path in the HR diagram from the region of red supergiants to the cool boundary of the Yellow Void over the last decade [13].

High-spectral-resolution monitoring of ρ Cas has been carried out on the 6-meter telescope of the Special Astrophysical Observatory since 2007. Spectroscopy of ρ Cas made on this telescope in 2007–2011 were analyzed and presented in [14]. Observations over a wide range of wavelengths with spectral resolution $R \geq 60\,000$ have enabled detailed studies of features in the optical spectrum and the detection of previously unknown properties of the kinematic state of the extended stellar atmosphere. The heliocentric radial velocity derived from symmetric absorption lines of metals varies with an amplitude of about ± 7 km/s relative to the center-of-mass velocity of the system (the systemic velocity) $V_{\text{sys}} = -47$ km/s. This time variability is a consequence of low-amplitude pulsations of near-photospheric layers of the atmosphere. At some epochs, a velocity gradient is observed in deep layers of the stellar atmosphere. Klochkova et al. [14] found a weak stratification of the velocities in the stellar atmosphere for the first time, manifest as a difference of 3–4 km/s in the velocities measured from absorption lines of neutral atoms and ions. These authors also showed that the long-wavelength components of the splitted absorptions of Ba II, Sr II, Ti II, and other strong lines whose lower levels have low excitation potentials are distorted by a stationary emission in the short-wavelength wings of these components. These non-trivial monitoring results serve as a stimulus for continued spectral monitoring of ρ Cas. In addition, photometric monitoring of the star (AAVSO) indicates that a new ejection of matter occurred in 2013, during which the brightness of the star decreased by 0.5^m . This event occurred only 12 years after the previous one in 2000–2001. Thus, the ejections in ρ Cas are becoming more frequent. According to [5, 15], this may indicate that the star is approaching a crossing of the Yellow Void. This fact suggests the urgent need of further monitoring of ρ Cas.

Numerous data have been published for this star, including high-resolution spectral data, however current notions about the kinematic state of its extended, unstable atmosphere do not fit any one, generally accepted interpretation. Resolution of this question also requires long-term, high-quality observations. We present here results based on spectral monitoring in 2013–2017. Section 2 briefly describes the methods used in the observations and analysis of the data. Section 3 presents our results and compare them with earlier data. Main conclusions are presented in Section 4.

2. Observations, reduction and analysis of the spectra

New spectral data for ρ Cas were obtained at the Nasmyth focus of the 6-m telescope of the Special Astrophysical Observatory (SAO) of the Russian Academy of Sciences using the echelle spectrograph NES [16, 17]. The observation dates, Julian dates (JD), and recorded spectral ranges are listed in Table 1. Observations were made using a large format 2048×4608 E2V CCD42-90-dd CCD. To de-

crease light losses at the entrance slit of the spectrograph without loss of spectral resolution, the NES is equipped with a three-slices image scanner. Each spectral order in the image is repeated three times with a shift along the dispersion of the echelle grating [17]. The transition to the large-format CCD substantially broadened the simultaneously recorded wavelength interval: for instance, $\Delta\lambda 5400 \div 8479 \text{ \AA}$ in the spectrum of October 1, 2014 or $4697 \div 7782 \text{ \AA}$ in spectra obtained in 2017. The spectral resolution is $\lambda/\Delta\lambda \geq 60\,000$, and the signal to noise ratio is $S/N \geq 100$.

The extraction of the one-dimensional spectra from the two dimensional echelle frames was carried out using the modified [18] ECHELLE software of the MIDAS package. Tracks of cosmicray particles were removed via median averaging of two successively obtained spectra. The wavelength calibration was carried out using the spectrum of a Th–Ar lamp with a hollow cathode. Positional and spectrophotometric measurements in the one-dimensional extracted spectra were made using a modern version of the Dech20t package [19]. The instrumental match of the stellar spectra and the calibration spectrum was checked using telluric lines of O_2 and H_2O . The V_r values were checked using measurements of up to 70–80 lines in the spectra of ρ Cas. The rms error in the V_r values derived from narrow telluric absorption lines is $\leq 0.5 \text{ km/s}$ (the accuracy for a single line). The accuracy obtained for ρ Cas is somewhat worse due to broadening of the spectral lines by turbulence in the stellar atmosphere. The procedure used to measure the radial velocities V_r from the NES spectra and the main sources of errors are described in more detail in [20, 21].

Table 1. Heliocentric radial velocities of ρ Cas. $V_r(\text{sym})$, $V_r(\text{blue})$, $V_r(\text{red})$ and $V_r(\text{emis})$ are the average velocities derived from symmetric absorption lines, short-wavelength components, long-wavelength components of splitted absorption lines, and weak emission lines of metals. The numbers of lines used for the measurements are listed in parentheses.

Date JD 2450000+	$\Delta\lambda$, nm	V_r , km/s				
		sym	blue	red	emis	H α
02.02.2013 6326.29	392–698	-41.79 ± 0.06 (494)	-60.9 ± 0.4 (16)	-34.8 ± 0.3 (22)	-49.8 ± 0.3 (3)	–40.1
08.08.2014 6877.53	392–698	$-\mathbf{42.37 \pm 0.12}$ (226), -32.18 ± 0.14 (249)	-79.0 ± 0.2 (49), -59.4 ± 0.4 (20)	-33.2 ± 0.2 (43)	-50.2 ± 0.7 (3)	–60.3
01.10.2014 6931.57	540–848	-36.35 ± 0.14 (181)	-81.0 ± 0.5 (6)	-35.8 ± 0.4 (12)	-51.9 ± 0.5 (11)	–59.3
13.02.2017 7797.59	470–778	-39.61 ± 0.06 (447)	-67.7 ± 0.3 (13), -55.3 ± 0.1 (13)	-33.7 ± 0.3 (13)	-52.2 ± 0.2 (7)	–41.3
06.08.2017 7971.50	470–778	-50.79 ± 0.09 (374)	-66.7 ± 0.2 (18), -56.4 ± 0.3 (13)	-31.2 ± 0.3 (14)	-48.2 ± 0.6 (6)	–31.4
06.08.2017 7972.34	470–778	-50.60 ± 0.07 (396)	-67.1 ± 0.2 (25), -56.3 ± 0.2 (20)	-31.0 ± 0.3 (20)	-46.8 ± 0.1 (5)	–31.2
13.08.2017 7979.30	470–778	-49.51 ± 0.07 (349)	-66.9 ± 0.2 (21), -56.5 ± 0.3 (12)	-32.1 ± 0.3 (22)	-50.1 ± 1.0 (4)	–31.8
05.09.2017 8013.52	470–778	-47.85 ± 0.07 (355)	-67.0 ± 0.2 (28), -56.3 ± 0.2 (19)	-33.0 ± 0.3 (16)		–46.1

The value derived from the lines of ions on August 8, 2014 is shown in boldface.

3. Discussion of results

When analyzing the observations, we measured radial velocities using different types lines in the spectrum of ρ Cas selected in accordance with [14]: weak symmetric absorptions, components of splitted

absorption lines of metals, and the H α line with its variable absorption-emission profile. In addition to these types of lines, the radial velocities were also measured using the weak, narrow emission lines of metals listed in Table 2. All these types of spectral features were already described in the earliest studies of the spectrum of this star [8, 22]. Let us consider in more detail the properties of the profiles of the above types of lines and the measurement results.

3.1. Metallic emissions

The wide range of wavelengths recorded in the spectra of ρ Cas obtained on October 1, 2014 and February 13, 2017 enabled measurement of the positions of several reliably selected weak emission lines of Fe, Co, and Ni with low excitation potentials $\chi_{low} \leq 3$ eV (see Table 2). The average radial velocity derived from these emission lines, presented in Table 1, varies only slightly with time, and differs little from the systemic radial velocity $V_{sys} = -47$ km/s [24]. The metal emission lines have widths of about 10 km/s, appreciably exceeding the width of the spectrograph instrumental profile $\delta Vr \approx 5$ km/s. The small widths of these emission lines and the coincidence of $V(\text{emis})$ with the systemic velocity indicates that these lines are formed in an external, extended gas envelope, whose dimensions substantially exceed the photometric radius of the star. If this envelope is optically thin in these emission lines, their positions indicate the systemic velocity of the star. This value remains constant within our uncertainties, and the rate of expansion of the shell is several km/s. Emission lines are observed predominantly during periods when the stellar brightness is decreasing; this may indicate relative stability of the emission measure, observed against the background of the weakened photospheric spectrum. Measurements of the intensity of emission lines relative to the local continuum are not sufficient to draw conclusions about their variability, since the level of the continuum can vary.

Table 2. Emission lines of metals in spectra of ρ Cas obtained at different epochs. Excitation potentials of lines χ_{low} were taken from the VALD database [23]. Condently identified emission lines are marked by a “+”, and uncertain features by a “+:”. A sign – indicates the absence of a given feature.

Line	χ_{low}	1.10.2014	13.02.2017	06.08.2017	13.08.2017	05.09.2017
FeI 8047.617	0.85	+				
FeI 7912.866	0.86	+	+			
FeI 7748.269	2.94	+	+	–	–	–
NiI 7714.308	1.94	+	+	–	–	–
FeI 7583.788	3.02	+	+	+	+	–
NiI 7291.449	1.94	+	+	+	+	–
CoI 7052.870	1.96	–	+	+:	+:	–
CoI 6814.950	1.96	+:	+	+	+	+:
FeI 6574.240	0.99	–	+	+	+	+:
FeI 6498.950	0.96	–	+	+	–	–
FeI 6358.693	0.85	+	+	+	+	+
NiI 6108.107	1.67	–	+	–	–	–
FeI 5956.700	0.86	–	+	+	+	+

As follows from Table 2, shell emissions of metals are most numerous in spectra obtained after the deep brightness minimum in 2014. After the brightness maximum, closer to Autumn 2017, the relative intensity of the metal emissions has decreased, and some have become completely absent from the spectra. All shell emissions were also absent in our spectra obtained in 2007–2011. The variability of the emissions is illustrated in Fig. 1, which shows a fragment of the spectrum of ρ Cas for two observing dates. The time behavior of the emission lines is consistent with the previous description of Scheffer

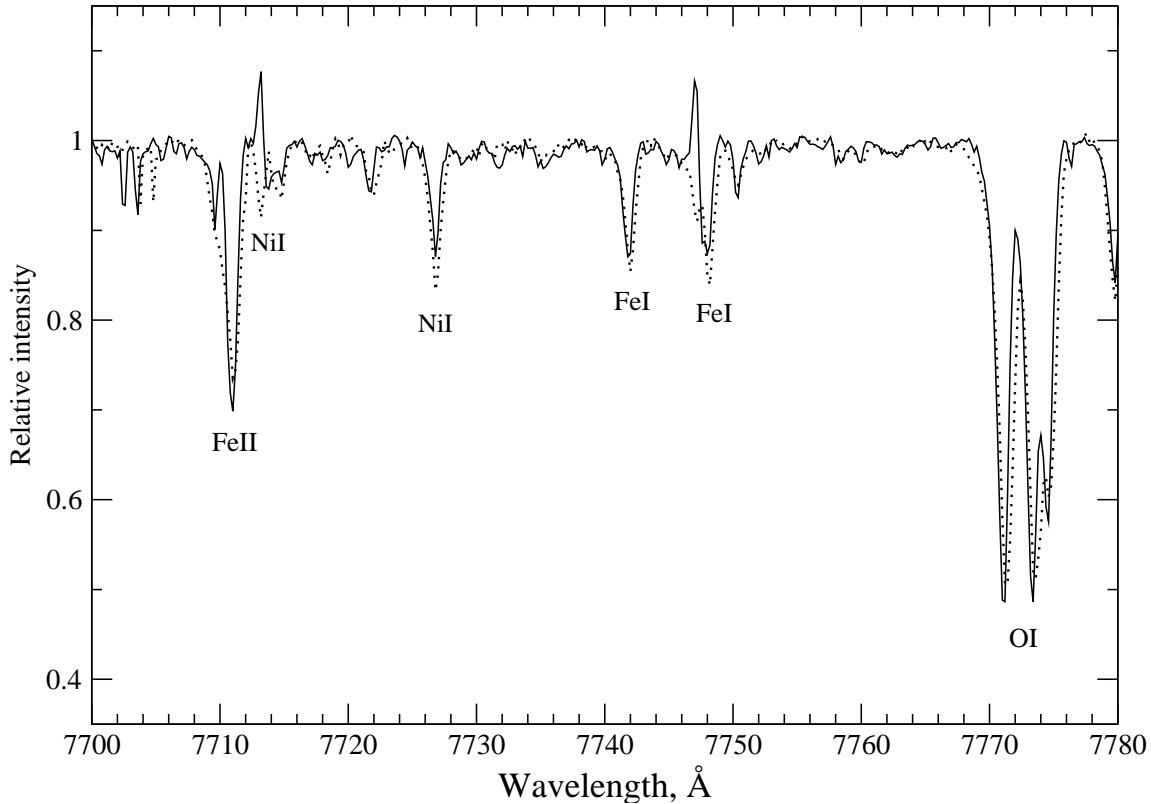


Figure 1. Fragments of the ρ Cas spectra at wavelengths 7696–7773 Å, obtained on February 13, 2017 (solid) and August 6, 2017 (dotted). The main identified absorption lines are marked. The fragment of the February 13, 2017 spectrum contains two weak emissions of NiI and FeI

and Lambert [25]. These authors, who obtained a large collection of spectra of ρ Cas, estimated the dominant period of stellar pulsations to be $\approx 500^d$.

Emissions of this type were also detected in the spectrum of ρ Cas earlier by Sargent [22] and Gorlova et al. [9]. All these authors also observed variability of weak emissions. Gorlova et al. [9] noted the appearance of emissions just after the brightness maximum, after which they weakened and disappeared as the brightness decreased. We have found a similar behavior of the emission lines in relation to the variability of the stellar brightness; as follows from the AAVSO database (www.AAVSO.org), both of our 2014 spectra and the spectrum for February 2017 were obtained when the brightness of ρ Cas was increasing. The spectra obtained in August–September 2017 correspond to the period of brightness decrease, when the intensity of the metallic emission lines was decreasing. A comparison of the data in Tables 2 and 1 shows that, at times when the largest numbers of emissions were detected (October 1, 2014 and February 2, 2017), the atmosphere was in the phase of compression: the radial velocity $V_r(\text{sym})$ differed by more than +10 km/s from the systemic velocity. Since August 2017, velocity $V_r(\text{sym})$ has been close to the systemic velocity and the intensity of the emissions has been decreasing, sometimes leading to their disappearance. It is obvious that the presence or absence of weak metal emissions depends on the flux level in the continuum. At times close to the maximum brightness, emissions are lost against the high flux background. The emissions become most intense during periods of powerful ejections of matter, which lead to weakening of the star brightness.

According to [26], the $H\alpha$ emission lines forms in the outer layers of the atmosphere, which are thermally excited by shocks. However, the observation of chromospheric effects in a star with such

a vigorous optically dense pseudo-photosphere as that of ρ Cas is unlikely. We attempted to search for traces of chromospheric emission in the core of the K line in the spectra taken on February 2, 2013 and August 8, 2014, where the recorded wavelength range includes the CaII resonant doublet. We confidently detected the remnants of the chromospheric emission profile for the low-luminosity objects, even at a level of 0.04 of the local continuum (see, e.g., Fig. 1a in [27]). However, in the spectrum of ρ Cas, only emissions of other metals with radial velocities close to the systemic velocity determined from the emission lines listed in Table 2 are observed against the background of the CaII line profile.

Since the stellar radiation in the cores of the resonance lines is more than 4^m weaker than the local continuum, emission lines of metals close to the cores of the CaII H and K lines are visible independent of the brightness variations of ρ Cas. For instance, no emission lines were present in the red part of spectrum of ρ Cas obtained on February 2, 2013, just before the ejection episode. However, on both this date and on August 8, 2014, we detected the CaII H and K lines in the short-wavelength part of the spectrum, in whose wings narrow metal emission lines originating in the shell are clearly visible, similar to those detected in the red part of the spectrum. The 6-th column of Table 1 lists the mean velocities $V(\text{emis})$ derived from the emission lines of FeI in the wings of the CaII H and K lines: 3927.92, 3930.30, and 3969.26 Å.

We emphasize that there is no emission in the cores of the CaII H and K lines, indicating the absence of a chromosphere, as it was noted earlier by Lobel et al. [5].

3.2. Behavior of the $H\alpha$ profile

For all observing dates in 2013–2017, the spectral interval recorded contains the $H\alpha$ line, whose complex absorption–emission profile is formed in high layers of the extended shell, which are affected by the stellar wind and shocks. As can be seen in Fig. 2, the position of the absorption core, the intensity of the emission components, and the ratio of their intensities vary with time. The variations of the position of the $H\alpha$ absorption core indicates that the region in which it is predominantly formed in the stellar atmosphere shifts. The type of the $H\alpha$ profile changed appreciably in the course of the new set of observations, as is clearly shown in Fig. 2.

In 2008–2011, the $H\alpha$ profile represented almost symmetric absorption with its core close to the systemic velocity, as in the $H\alpha$ profile in the spectrum taken on August 21, 2008 (Fig. 2). However, in the spectrum taken on February 2, 2013, even before the beginning of the shell episode, the $H\alpha$ profile shifted toward longer wavelengths, indicating the onset of the collapse of the atmospheric layers in which this line forms. Just after the shell episode, on October 1, 2014, the profile again changed significantly: the line has a doubled core whose short-wavelength component is shifted by up to 50 km/s respective to the systemic velocity. In 2017, the $H\alpha$ line resembled an inverse P Cygni profile (February 13, 2017). It then again became doubled, with a large shift, but this time toward longer wavelengths (August 6, 2017). This testifies to a contraction of the upper layers of the atmosphere. This behavior of the $H\alpha$ profile indicates increased instability of the upper layers of the stellar atmosphere before the ejection and during the restoration of the brightness following this episode.

Dates of observations when significant $H\alpha$ emission appears are of the most interest. In our new set of spectra, emission (at $\approx 20\%$ of the continuum level) was detected on February 2, 2013 and on February 13, 2017. Both profiles are shown in Fig. 2. As follows from the AAVSO data, both observing moments correspond to the ascending branch, before the maximum brightness. One of the spectra of our earlier set (years 2007–2011) is of particular interest. As can be seen in Fig. 1 of [14], in the spectrum for October 20, 2008, emission features were detected in both wings of the $H\alpha$ line. This epoch corresponds to the descending branch of the light curve.

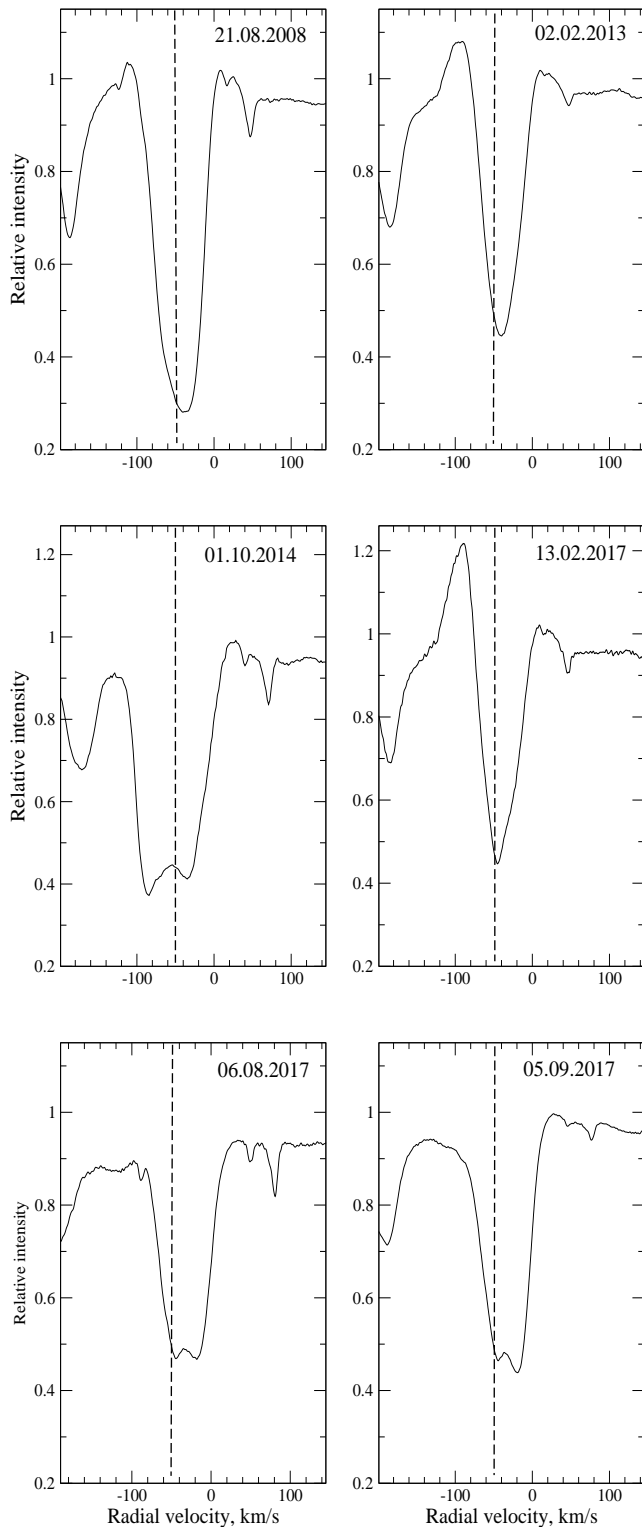


Figure 2. H α profile in spectra of ρ Cas obtained on different dates. The vertical dashed line shows the systemic velocity $V_{\text{sys}} = -47$ km/s [24].

The appearance of $H\alpha$ emission is not related to the properties of the metal-line profiles on these dates. As can be seen from the data in Table 1, the profiles of strongest absorptions have two components in the spectrum for February 2, 2013, while they have three components in the spectrum for February 13, 2017 and subsequent dates. On the other hand, the $H\alpha$ line has different profiles on February 13, 2017 and August 6, 2017, while the velocity patterns and strongest absorption profiles for these two spectra coincide. The velocities derived from weak symmetric absorption lines also differ on these dates. Thus, we have found new evidence for an absence of a direct link between the layers in which $H\alpha$ and strongest absorptions are formed and deeper layers that are subject to pulsations.

3.3. Split absorptions

In the spectra taken on all dates in 2014 and 2017, the profiles of strong absorptions in the spectrum of ρ Cas remained splitted. A list of splitted absorptions in the spectra of ρ Cas was presented earlier in [14]. The short-wavelength components of the splitted absorptions are formed in the uppermost layers of the expanding atmosphere, close to the circumstellar gaseous envelope, as is confirmed by the coincidence of the velocities of these components and those derived from CO lines [8]. However, unlike earlier observing seasons (2007–2011), the strongest absorptions in the 2017 spectra have a more complex structure, since the short-wavelength component also displays two absorption features. This is clearly visible in Fig. 3, where the profile of the strong BaII 6141 Å absorption line observed on February 13, 2017 is compared to profiles of this line from earlier observing seasons (2008 and 2013) in a plot of radial velocity versus relative intensity. It is necessary to emphasize that the long-wavelength component displays a constant shift relative to the systemic velocity by approximately 15 km/s.

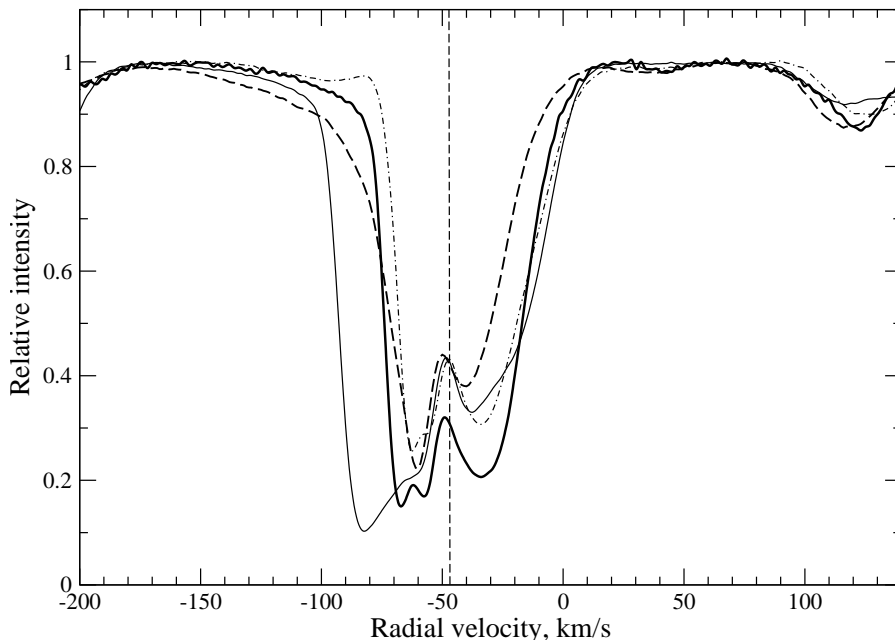


Figure 3. Profiles of the BaII 6141 Å line in the spectra of ρ Cas for September 30, 2009 (dash-dot), February 2, 2013 (dashed), August 8, 2014 (thin solid), and February 13, 2017 (bold). The vertical dashed line shows the systemic velocity $V_{\text{sys}} = -47$ km/s [24].

The kinematic instability of the upper atmospheric layers subject to the influence of the stellar wind is also manifest as variability of the short-wavelength wing of the BaII 6141 Å line, which indicates appreciable strengthening of the wind before the shell ejection, as can be seen in the spectrum taken

on February 2, 2013 in Fig. 3, even before the shell episode extends to -150 km/s. In the spectrum for August 8, 2014, during the exit from the minimum state, the shape of the BaII 6141 Å profile differs significantly from its shape at the other epochs shown in Fig. 3. The line is still splitted, and the position and intensity of the long-wavelength component does not differ from their values in the profile at earlier times. The short-wavelength component is considerably broadened (by approximately a factor of two), and is also shifted toward shorter wavelengths, as can also be seen from the data presented in Table 1.

The BaII 6141 Å profiles in Fig. 3 illustrate well the difference in the steepness of the wings of the two components of the splitted absorption, indicating different profile widths and differences in the physical conditions in the regions of formation of the components. This confirms that the short-wavelength component with its steeper short-wavelength wing is formed in uppermost layers of the extended stratified atmosphere of the hypergiant. Additional splitting of the short-wavelength component indicates intensified stratification of the uppermost layers of the atmosphere.

3.4. New traits of the kinematic state of the atmosphere of ρ Cas

All our radial-velocity measurements using lines of different types are presented in Table 1 and in several figures showing profiles of various spectral features. The amplitude of the velocity variability we have derived from symmetric absorption lines, $V_r(\text{sym})$, exceeds 10 km/s, which is higher than the variability amplitude found in our previous study of ρ Cas. The V_r values for the short-wavelength components $V_r(\text{blue1})$ and $V_r(\text{blue2})$ presented in Table 1 differ by more than 12 km/s. As follows from Fig. 3, this splitting of the line, which was absent from all previous spectra [14, Fig. 1], is already appreciable in the spectrum taken on September 30, 2009.

Figure 4 can be used to compare the behavior of the profiles of $H\alpha$ and the splitted absorptions. In the 2014 spectrum, before the appearance of $H\alpha$ emission, the position and width of the profile of this line almost coincided with those for the splitted absorptions. At the epoch when the emission appears (February 13, 2017), the shift of the shortest-wavelength component of the splitted absorptions toward shorter wavelengths decreases to $V_r(\text{blue}) \approx -67$ km/s. As can be seen from the fourth column of Table 1, on subsequent dates, this short-wavelength component and the entire BaII 6141 Å profile remain at the same position, independent of the continuing variations of the $H\alpha$ profile. In general, we conclude that there is no strict correlation between the evolution of the $H\alpha$ and BaII 6141 Å profiles. For all the dates in Fig. 4, the vertical bar indicates the value of $V_r(\text{sym})$ derived from symmetric absorptions. Figure 4 shows an absence of any relationship between the position of the $H\alpha$ line and $V_r(\text{sym})$; i.e., pulsations in deep layers of the atmosphere do not affect the $H\alpha$ profile, which forms in high atmospheric layers.

It is surprising that the positions of strong absorptions were continuously stable. This is clearly visible in the BaII 6141 and FeI 5446 Å profiles in Fig. 4, and the positions of both the long- and short-wavelength components for a large set of splitted absorptions in Table 1. This result is also confirmed by the positions of the long- and short-wavelength components in 2007–2011 [14]. However, the positions of the short-wavelength components of the splitted absorptions is subject to the influence of the stellar wind, manifest as a distortion of the short-wavelength wings of these lines. In essence, we can conclude that the strongest atmospheric absorptions are not influenced by pulsations.

A special velocity pattern was obtained in the spectrum taken on August 8, 2014, at the maximum brightness of the star. Measurements of a large set of symmetric absorptions in this spectrum demonstrate a systematic difference between the velocities derived from absorption lines of ions and neutral atoms, by about 10 km/s. This kind of stratification was found by us earlier for several observations of ρ Cas in 2007–2011 (see [14, Fig. 2]). However, this velocity difference is particularly large in the spectrum for August 8, 2014: $V_r(\text{sym}) = -42.37$ km/s for ions, while $V_r(\text{sym}) = -32.18$ km/s for neutral

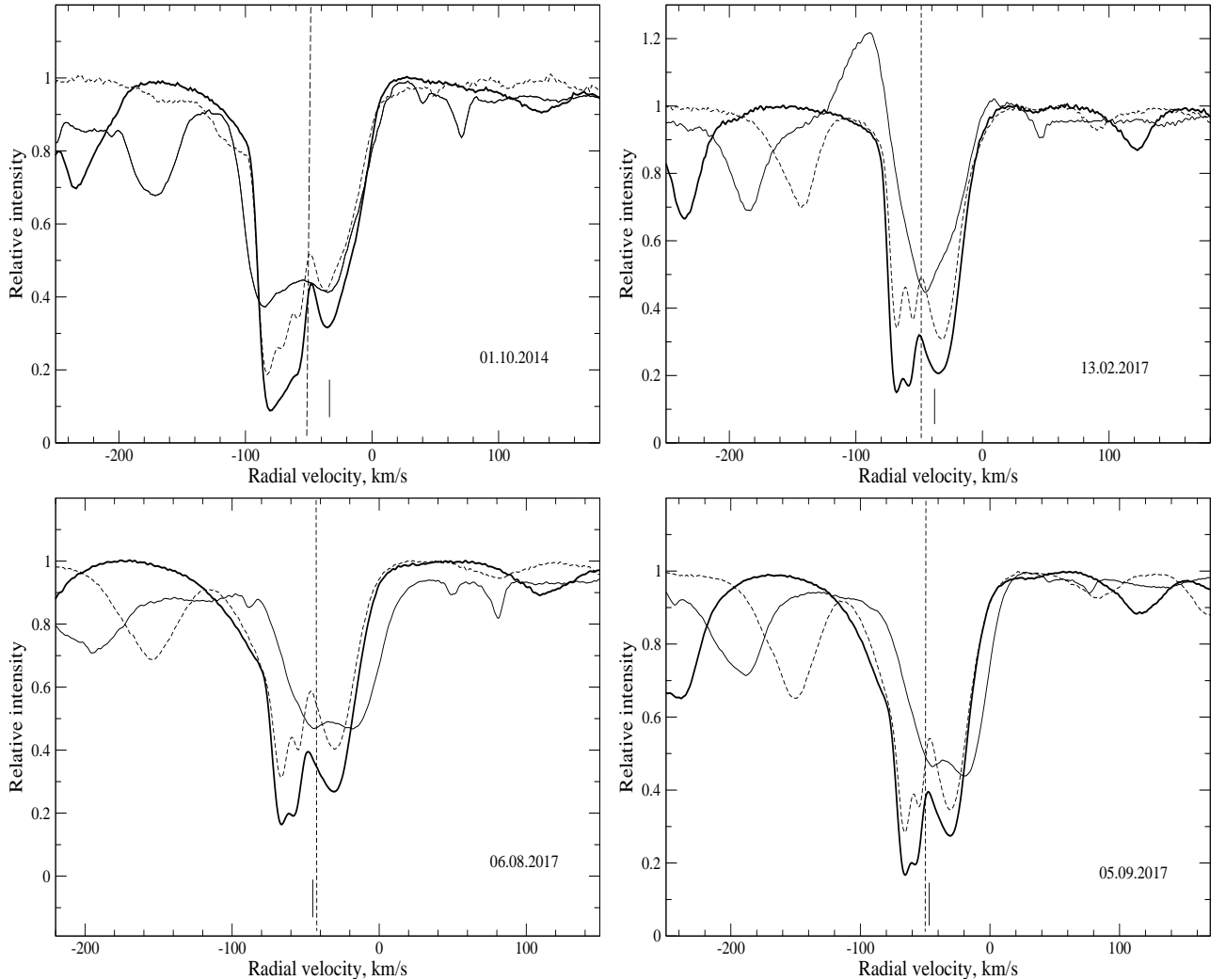


Figure 4. Diversity of the profiles of selected lines in the spectra of ρ Cas: $H\alpha$ (thin), FeI 5446 (dashed), and BaII 6141 (bold). The vertical dashed line shows the systemic velocity $V_{\text{sys}} = -47$ km/s [24]. In all panels, the vertical bar indicates the velocity derived from symmetric absorption lines (see Table 1).

atoms. The difference of the radial velocities derived from symmetric absorptions of ions and atoms is also visible in Fig. 5.

To increase the time interval for comparing the behavior of the radial velocities measured from symmetric absorptions $V(\text{sym})$ and $H\alpha$, we added the results of [14], obtained using the same spectrograph and method, to Fig. 5. Figure 5 shows that $V(\text{sym})$ and $V(H\alpha)$ do not agree for most of the observations. We emphasize that, contrary to the claim of Lobel et al. [24], these velocities turned out to be close or coincident at several epochs. The velocity differences obtained using observations obtained on the same date indicate a dynamic stratification of the upper atmospheric layers of ρ Cas.

The difference between $V(\text{sym})$ and $V(H\alpha)$ is particularly large in August–September 2017, on the descending branch of the brightness variations. At the same time, $V(\text{sym})$ and $V(H\alpha)$ agree in the spectra taken on February 2, 2013 and February 13, 2017, on the rising branch of the brightness variations. However, these velocities differ strongly in spectra taken on the rising branch in 2014. It is interesting that the unusual $H\alpha$ profile with emission in the line core also first appeared in 2014. It is not by chance that this unique profile of splitted absorptions and additional velocity stratification

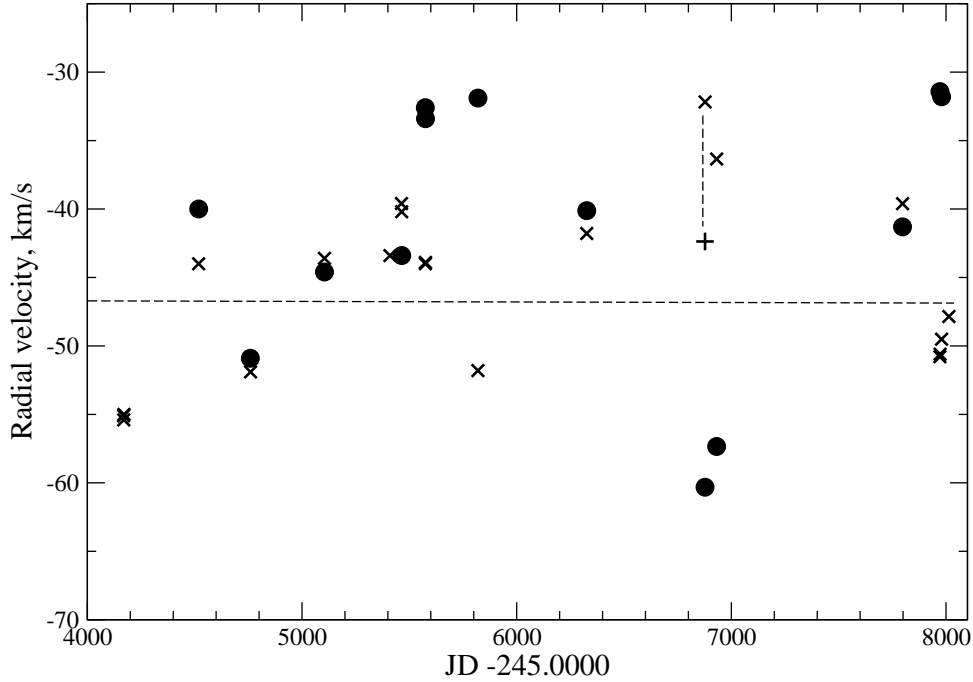


Figure 5. Behavior of the radial velocities measured from symmetric absorption lines (xs) and the $H\alpha$ line (bold points) in the spectrum of ρ Cas. Data for epochs preceding JD 2456300 were taken from [14]. The vertical dashed line connects the velocities measured on August 8, 2014 using symmetric absorptions of ions (plus) and neutral atoms (x).

indicated by lines of ions and neutral atoms was first detected on August 8, 2014. These changes are obviously due to the fairly powerful ejection ($\approx 0.5^m$) that occurred from April to November 2013, when the effective temperature of the star decreased from 7000 to 5000 K [15]. As it can be seen from our spectrum for February 2, 2013, before the beginning of this shell episode, the stellar spectrum and the velocity pattern in the atmosphere corresponded to the data for 2007–2011 [14].

At certain epochs, the velocities measured from absorption lines of ions with high excitation potentials differ significantly from those derived from other absorption lines. Such absorption lines include SiII 4028, 4128, 5041, 5055, and 5056 Å, for which the excitation potentials of the lower level is about 10 eV, SiII 6347 and 6371 Å, for which the excitation potentials of the lower level is about 8 eV, and some lines of FeII, for which the excitation potentials of the lower level above 5 eV: FeII 6383, 6443, 6446 Å. The velocities derived from these high-excitation absorption lines, which form in the deepest layers of the atmosphere, is always close to the systemic velocity.

The profiles of the NaI D lines (Fig. 6) contain broad components, similar to those possessed by the strongest absorptions, but broader, as well as a narrow absorption feature with $V_r = -49.8$ km/s and another component close to $V_r \approx -29$ km/s that is poorly distinguished in our spectra. The absorption with $V_r \approx -50$ km/s is formed in the interstellar medium, and indicates a position for ρ Cas beyond the Perseus arm [28]. The interstellar NaI line corresponding to the Local Arm cannot be distinguished in the long-wavelength photospheric component. The features observed in the KI 7698 Å profile shown in Fig. 6 mainly correspond to those of the NaI D lines. However, interstellar components with $V_r \approx -12$ and -29 km/s, corresponding to the Local Arm and Perseus Arm, are clearly distinguished in the former. Figure 6 also shows the BaII 6141 Å profile, providing additional support for our conclusion

in [14] that the short-wavelength components of splitted absorptions form in the circumstellar medium of the hypergiant.

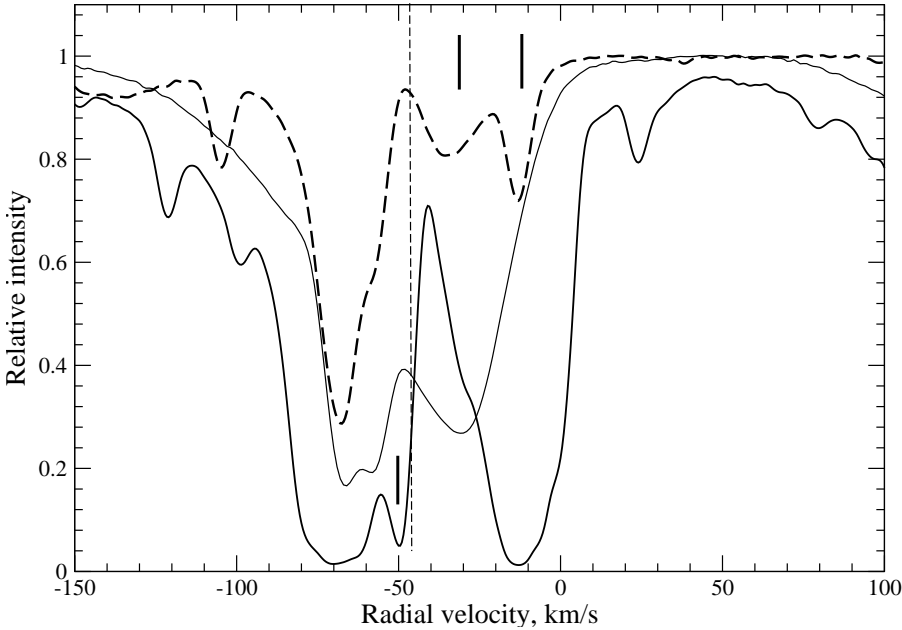


Figure 6. Profiles of selected lines in the spectrum of ρ -Cas obtained on August 6, 2017: D2 NaI 5889 Å (bold), KI 7698 Å (dashed), and BaII 6141 Å (thin). The vertical bars mark the positions of interstellar lines with velocities $V(\text{IS}) = -49.7$, -29 , and -12 km/s. The vertical dashed line indicates the systemic radial velocity $V_{\text{sys}} = -47$ km/s [24].

We should make one more remark about the radial velocities measured using emission and absorption lines. For absorptions that form close to the photosphere and show low-amplitude pulsations, it is fair to assume that the radial velocity of the pulsating layers can be obtained by multiplying the measured velocity by a projection factor p that depends on the adopted limb-darkening law. This factor also differs for various model approximations; for instance, $p = 1.41$ [29] and 1.31 [30]. Consequently, in the translation from the measured radial velocities to the velocities of the motion along the radius, all values derived from absorptions of moderate intensity (about ± 10 km/s) should be multiplied by a projection factor p . In this case, the amplitude of the pulsation radial velocity will increase to $\pm 13 \div 14$ km/s. This correction does not apply to emission lines formed in the outer, diluted shell, where the same contributions to the profile are made by the near and far hemispheres relative to the observer. Figures 2, 3, 4, and 6 compare the observed profiles on the scale of the measured radial velocities, and therefore velocities corresponding to the positions of the absorption wings of the lines should be increased by a factor of 1.3. In this case, the pattern of the motions becomes more realistic: outward motions dominate over the systemic velocity. However, the emission details of the $\text{H}\alpha$ line form under conditions intermediate between the outermost comparisand deep layers of the atmosphere. Therefore, strictly speaking, the shape of any complex emission-absorption profile should change upon recalculation to velocities of the motion along the radius. This also applies to the case when the splitting of strongest absorptions of metals is interpreted as the result of the appearance of an emission feature in the core of the absorption line [5], with the position of this emission feature coinciding with the systemic velocity. If we believe that the emission in lines of metals arises in a region of emitting behind a shock front, so that we observe emission only from the near hemisphere, we must explain this surprising coincidence of velocities. In addition, the splitting of absorptions into

three components that we have found in this study does not fit into a picture with the formation of a shock front that is at rest relative to the center of the star.

4. Conclusions

We have presented the results of an analysis of optical spectra of ρ Cas obtained shortly before and just after its brightness minimum in 2013. Various lines in the spectra of this star, which has an extremely extended atmosphere, are variable and always show differential shifts, since the regions of their formation extend from pulsating near-photospheric layers to the non-stationary wind. We have found that the velocity derived from symmetric absorption lines $V_r(\text{sym})$ is variable, with an amplitude of more than 10 km/s higher than the amplitude found in our previous study of ρ Cas.

Continuation of spectral monitoring using homogeneous material has led to the discovery of new phenomena. This is also true of the behavior of the $H\alpha$ line. While the $H\alpha$ had an almost symmetric absorption profile with the position of the core close to the systemic velocity in 2008–2011, this profile changed substantially after the shell episode, starting from October 1, 2014, when the line acquired a doubled core, with the short-wavelength component shifted by up to 50 km/s relative to the systemic velocity. At different observing dates in 2017, the $H\alpha$ had an inverse P Cygni profile (February 13, 2017) and a doubled profile with a large offset toward longer wavelengths (August 6, 2017). These shifts of the $H\alpha$ profile indicate changes in the structure of the upper layers of the extended atmosphere and enhanced instability of these layers. The shift of the profile towards longer wavelengths indicates an infall of the layers where the line is formed.

A comparison of the radial velocities derived from symmetric absorption lines and from the $H\alpha$ line shows that these velocities disagree for most epochs, indicating inhomogeneity of the upper layers of the atmosphere and gaseous envelope of the star. This difference is particularly large in spectra obtained on the descending branch of the brightness. The velocities $V(\text{sym})$ and $V(H\alpha)$ agree in the spectra obtained on February 2, 2013 and February 13, 2017, when the brightness was increasing. However, $V(\text{sym})$ and $V(H\alpha)$ differ considerably in the 2014 spectra, obtained on the rising branch of the brightness variations, when the doubled core of $H\alpha$ appeared for the first time. In a spectrum obtained on August 8, 2014, we found additional stratification of the velocities derived from lines of ions and neutral atoms.

In the long-wavelength region of the spectrum, we identified several weak shell emission lines of iron group elements in the spectrum taken in 2013; the intensity of these emissions decreased in 2017, with only a small fraction being visible in the spectrum for September 5, 2017. Shell emission lines of metals were also detected in the wings of the H and K lines of CaII.

The profiles of strongest absorptions remained splitted in all spectra of ρ Cas obtained in 2014 and 2017. However, unlike the previous observing seasons, these absorptions have three rather than two components in the 2017 spectra. This new property of the splitted absorptions supports our interpretation of this structure: the short-wavelength components of these lines is formed in the circumstellar envelope, where weak emissions of metals and one of the broad components of the NaI D doublet are also formed.

The kinematic instability of the upper atmosphere, which is subject to the influence of the stellar wind, is manifest via the variability of the short-wavelength wing of the BaII 6141 Å line, which extends to -150 km/s in the spectrum taken on February 2, 2013, before the mass ejection event. In general, we observe that the atmosphere of ρ Cas has experienced the influence of an additional factor during the ejection episode, which substantially changed the kinematic pattern of its upper layers.

Acknowledgements

This study was supported by the Russian Foundation for Basic Research (grants 16–02–00587 a and 18–02–00029 a). We have made use of the SIMBAD, SAO/NASA ADS, and VALD databases.

References

1. C. de Jager, *Astron. Astrophys.* **8**, 145 (1998).
2. C. de Jager, A. Lobel, H. Nieuwenhuijzen, and R. Stothers, *Mon. Not. R. Astron. Soc.* **327**, 452 (2001).
3. R. M. Humphreys, *Rev. Mex. Astron. Astrofis.* **30**, 6 (2007).
4. Yu. A. Fadeev, *Astron. Lett.* **37**, 403 (2011).
5. A. Lobel, A. K. Dupree, R. P. Stefanik, G. Torres, et al., *Astrophys. J.* **583**, 923 (2003).
6. D. Shenoy, R. M. Humphreys, T. J. Jones, M. Marengo, et al., *Astron. J.* **51**, 51 (2016).
7. M. Schuster, R. M. Humphreys, and M. Marengo, *Astron. J.* **131**, 603 (2006).
8. D. L. Lambert, K. H. Hinkle and D. N. B. Hall, *Astrophys. J.* **248**, 638 (1981).
9. N. Gorlova, A. Lobel, A. G. Burgasser, J. H. Rieke, I. Llyin, and J. P. Stauffer, *Astrophys. J.* **651**, 1130 (2006).
10. V. Klochkova, E. Chentsov, and V. Panchuk, *Mon. Not. R. Astron. Soc.* **292**, 19 (1997).
11. R. D. Oudmaijer, *Astron. & Astrophys. Suppl. Ser.* **129**, 541 (1998).
12. V. G. Klochkova, M. V. Yushkin, E. L. Chentsov, and V. E. Panchuk, *Astron. Rep.* **46**, 139 (2002).
13. V. Klochkova, E. Chentsov, A. S. Miroshnichenko, V. E. Panchuk, and M. V. Yushkin, *Mon. Not. R. Astron. Soc.* **459**, 4183 (2016).
14. V. G. Klochkova, V. E. Panchuk, N. S. Tavalzhanskaya, and I. A. Usenko, *Astron. Rep.* **58**, 101 (2014).
15. A. Aret, M. Kraus, I. Kolka, and G. Maravelias, in *The B[e] Phenomenon: Forty Years of Studies*, Ed. by A. Miroshnichenko, S. Zharikov, D. Korčáková, M. Wolf, *ASP Conf. Ser.* **508**, 357 (2017).
16. V. E. Panchuk, V. G. Klochkova, M. V. Yushkin, and I. D. Najdenov, *J. Opt. Technol.* **76**, 42 (2009).
17. V. E. Panchuk, V. G. Klochkova, and M. V. Yushkin, *Astron. Rep.* **61**, 820 (2017).
18. M. V. Yushkin and V. G. Klochkova, *SAO Preprint No. 206 (Spec. Astrophys. Observ., Russia, 2004)*.
19. G. A. Galazutdinov, *SAO Preprint No. 92 (Spec. Astrophys. Observ., Russia, (1992))*.
20. V. G. Klochkova, V. E. Panchuk, M. V. Yushkin, and D. S. Nasonov, *Astrophys. Bull.* **63**, 386 (2008).
21. V. G. Klochkova and N. S. Tavganskaya, *Bull. Spec. Astrophys. Observ.* **65**, 18 (2010).
22. W. L. W. Sargent, *Astrophys. J.* **134**, 142 (1961).
23. N. E. Piskunov, F. Kupka, T. A. Ryabchikova, W. W. Weiss, and C. S. Jeffery, *Astron. Astrophys. Suppl. Ser.* **112**, 525 (1995).
24. A. Lobel, G. Israelian, C. de Jager, F. Musaeu, J. W. Parker, and A. Mavrogiorgou, *Astron. & Astrophys.* **330**, 659 (1998).
25. Ya. Sheffer and D. L. Lambert, *Publ. Astron. Soc. Pacif.* **98**, 914 (1986).
26. C. de Jager, A. Lobel, and G. Israelian, *Astron. & Astrophys.* **325**, 714 (1997).
27. V. E. Panchuk, V. G. Klochkova, and M. V. Yushkin, *Astrophys. Bull.* **65**, 269 (2010).
28. Y. P. Georgelin and Y. M. Georgelin, *Astron. & Astrophys.* **6**, 349 (1970).
29. E. A. Milne, *Mon. Not. R. Astron. Soc.* **94**, 418 (1934).
30. S. B. Parsons, *Astrophys. J.* **174**, 57 (1972).